Cancer-associated mutations in the p85α N-terminal SH2 domain activate a spectrum of receptor tyrosine kinases

Xinran Li[a], Amy Y. T. Lau[a], Angel S. N. Ng[a,1], Abdullah Aldehaiman[b,1], Yuan Zhou[a], Patrick K. S. Ng[c,2], Stefan T. Arold[b,d,3], and Lydia W. T. Cheung[a,3]

[a]School of Biomedical Sciences, Li Ka Shing Faculty of Medicine, The University of Hong Kong, Hong Kong; [b]Biological and Environmental Science and Engineering, Computational Bioscience Research Center, King Abdullah University of Science and Technology, Thuwal 23955-6900, Saudi Arabia; [c]Institute for Personalized Cancer Therapy, The University of Texas MD Anderson Cancer Center, Houston, TX 77030; and [d]Centre de Biologie Structurale, INSERM, Université de Montpellier, Montpellier 34090, France

Edited by Joan S. Brugge, Harvard Medical School, Boston, MA, and approved July 2, 2021 (received for review January 29, 2021)

The phosphoinositide 3-kinase regulatory subunit p85α is a key regulator of kinase signaling and is frequently mutated in cancers. In the present study, we showed that in addition to weakening the inhibitory interaction between p85α and p110α, a group of driver mutations in the p85α N-terminal SH2 domain activated EGFR, HER2, HER3, c-Met, and IGF-1R in a p110α-independent manner. Cancer cells expressing these mutations exhibited the activation of p110α and the AKT pathway. Interestingly, the activation of EGFR, HER2, and c-Met was attributed to the ability of driver mutations to inhibit HER3 ubiquitination and degradation. The resulting increase in HER3 protein levels promoted its heterodimerization with EGFR, HER2, and c-Met, as well as the allosteric activation of these dimerized partners; however, HER3 silencing abolished this transactivation. Accordingly, inhibitors of either AKT or the HER family reduced the oncogenicity of driver mutations. The combination of these inhibitors resulted in marked synergy. Taken together, our findings provide mechanistic insights and suggest therapeutic strategies targeting a class of recurrent p85α mutations.

p85α | receptor tyrosine kinases | mutation

PIK3R1, which encodes the p85α regulatory subunit of phosphoinositide 3-kinases (PI3Ks), is frequently mutated in cancers. *PIK3R1* mutations are associated with poor survival of cancer patients [the Genomic Data Commons (GDC) Data Portal] (1). Cancer-associated mutations have been detected in all five protein domains of p85α, namely, the Src homology 3 (SH3) domain, GTPase-activating protein (GAP) domain, N-terminal SH2 (nSH2) domain, inter-SH2 (iSH2) domain, and C-terminal SH2 (cSH2) domain (2). Hotspot *PIK3R1* mutations cluster in the iSH2 and SH2 domains in agreement with the primary roles of these domains in stabilizing and inhibiting p110 in the p85α–p110 heterodimer (3).

The first reported and characterized clusters of cancer patient–derived mutations were located in two regions of the iSH2 domain (i.e., the E439–K459 and D560–W583 regions) (4–6). Driver mutations in these regions can disrupt the inhibitory interaction between the iSH2 and p110 C2 domains (7), thereby alleviating the inhibition of p110 kinase activity by p85α (8). The other driver mutations target the inhibitory interactions between the nSH2 domain and p110 helical domain (9). The nSH2 domain driver mutations (G376R and K379E) have been suggested to play oncogenic roles by weakening this inhibitory interface (4). Importantly, all these p85α mutants retain the ability to physically bind to p110 and stabilize it. The cSH2 domain interacts with the p110 kinase domain and contributes to p110 inhibition (10). A cSH2 domain driver mutation, K674R, elevates AKT phosphorylation (11). However, the effect of this mutant on p110 remains to be elucidated. Apart from binding to p110, the nSH2 and cSH2 domains bind to phosphotyrosine (pY)-containing consensus sequences (pYXXM) in pY-phosphorylated receptor tyrosine kinases (RTK) or adaptor proteins (3). Engineered p85α mutations in the nSH2 (R358A, S361D) and cSH2 (R649A, S652D) domains impair binding to pY peptides by either removing charge pairing (R358A and R649A) or introducing charge repulsion (S361D, S652D) to the pY phosphate group (12, 13). Binding to the pY motifs upon RTK stimulation is incompatible with the p110-inhibiting interactions of the p85α SH2 domains. Therefore, binding of p85α to pY motifs allows the controlled activation of p110.

In this study, we revealed an oncogenic mechanism evoked by a group of driver mutations in the nSH2 domain. These p85α mutations promote the stabilization of the HER3 protein, thereby activating multiple RTKs. The activation of both RTKs and PI3K/AKT by these nSH2 domain driver mutations should be considered to achieve therapeutic efficacy.

Results

nSH2 Domain Driver Mutations Promote Malignant Phenotypes In Vitro and In Vivo. A previous functional genomic screen annotated 12 patient-derived *PIK3R1* mutations in the nSH2 domain (14). Ten of these mutations were oncogenic that promoted the

Significance

Phosphoinositide 3-kinase activation typically occurs following stimulation by upstream receptor tyrosine kinases (RTKs), which alleviate p110α inhibition by p85α. p85α and p110α driver mutations have been reported to activate p110α by disrupting the inhibitory interface between p85α and p110α. This study revealed that driver mutations in the p85α N-terminal SH2 domain can enhance p110α activity by inducing the activation of multiple RTKs. Furthermore, combination treatment with RTK and AKT inhibitors provides synergistic therapeutic efficacy. This previously uncharacterized oncogenic mechanism presents the exploitable vulnerability of a class of p85α mutant tumors.

Author contributions: X.L., S.T.A., and L.W.T.C. designed research; X.L., A.Y.T.L., A.S.N.N., A.A., Y.Z., S.T.A., and L.W.T.C. performed research; P.K.S.N. contributed new reagents/analytic tools; X.L., A.Y.T.L., A.S.N.N., A.A., P.K.S.N., S.T.A., and L.W.T.C. analyzed data; and A.Y.T.L., S.T.A., and L.W.T.C. wrote the paper.

The authors declare no competing interest.

This article is a PNAS Direct Submission.

[1]A.S.N.N. and A.A. contributed equally to this work.

[2]Present address: The Jackson Laboratory for Genomic Medicine, Farmington, CT 06032.

[3]To whom correspondence may be addressed. Email: stefan.arold@kaust.edu.sa or lydiacwt@hku.hk.

This article contains supporting information online at https://www.pnas.org/lookup/suppl/doi:10.1073/pnas.2101751118/-/DCSupplemental.

Published September 10, 2021.

survival of growth factor–dependent cells in the absence of a growth factor (*SI Appendix*, Fig. S1*A*). The remaining two mutations were functionally neutral passengers. Among the 10 driver mutations, four were truncated mutants that do not bind to p110 and have acquired a neomorphic function of activating the MAPK pathways (15). In this study, we characterized the other six driver mutations, namely, W333R, G353R, LR372del, G376R, K379E, and L380del. Endometrial cancer cells were used as models, because 1) endometrial cancer patients with *PIK3R1* mutations had significantly worse survival outcomes than patients with wild-type (WT) *PIK3R1* ($P = 0.035$; *SI Appendix*, Fig. S1*B*) (1), and 2) nSH2 domain mutations are frequent in the disease.

To assess the functional consequences driven by the six nSH2 domain mutations, endometrial cancer cells KLE and EFE-184 stably expressing WT or mutant *PIK3R1* were subjected to the cell viability and colony formation assays. The passenger mutation R386G was used as the control. The KLE and EFE-184 cells harbored WT *PIK3R1* and genes of the major members of the PI3K pathway. Overexpression of HA-tagged p85α WT and mutants was confirmed (*SI Appendix*, Fig. S1*C*). Cells stably expressing LacZ were included as a control. Consistent with the initial screening, we observed marked increases in the cell viability and clonogenic growth capacity of cells expressing W333R, G353R, LR372del, G376R, K379E, or L380del compared with those expressing *PIK3R1* WT or the passenger R386G (Fig. 1 *A* and *B*). In addition to cell growth, the six driver mutations significantly enhanced cell migration (Fig. 1*C* and *SI Appendix*, Fig. S1*D*) and invasion (Fig. 1*D* and *SI Appendix*, Fig. S1*E*). To investigate the effect of the driver mutations on tumorigenic progression in vivo, the EFE-184 stable cells were subcutaneously injected into female nude mice. The weights of the tumors expressing the driver mutations were significantly higher than those of the tumors expressing WT *PIK3R1* or the passenger R386G (Fig. 1*E*).

p110α and the AKT Pathway Are Activated by nSH2 Domain Driver Mutations. We investigated the physical association between the p85α nSH2 domain driver mutations and p110α. Consistent with the notion that the interaction between p85α and p110 is primarily mediated by the iSH2 domain, all p85α nSH2 domain mutants could bind to p110α in immunoprecipitation experiments using anti-HA or anti-p110α antibody (Fig. 2*A* and *SI Appendix*, Fig. S2). The physical association between p85α and p110α protects p110α from degradation (16). Accordingly, we observed elevated p110α protein levels in WT p85α-overexpressing cells than LacZ-expressing cells (Fig. 2*B*). Elevated p110α levels were found in cells expressing all mutations, including the passenger, suggesting that the mutations do not disrupt the physical association of p85α with p110α.

In the PI3K heterodimer, inhibitory contacts are present between the p85α nSH2 domain and p110 helical domain (9). To examine whether nSH2 domain driver mutations altered p110α kinase activity, we measured the production of phosphatidylinositol 3,4,5 trisphosphate (PIP3) catalyzed by immunoprecipitated p110α. p110α exhibited higher kinase activity in the presence of oncogenic mutants (Fig. 2*C*), with concomitant increase in PIP3 levels (Fig. 2*D*). G376R, K379E, and L380del are located on the β-strand 3 that is in direct contact with p110α. These mutations compromise the inhibitory association of nSH2 with p110α, explaining the increased p110α activity (8). W333R, G353R, and LR372del are expected to destabilize the three-dimensional structure of nSH2 and thereby its association with p110α, through the loss of hydrophobic interactions and the introduction of clashes, strains, and unfavorable charges (*SI Appendix*, Fig. S3*A*). Differential scanning fluorimetry (DSF) on purified recombinant nSH2 domains confirmed that W333R, G353R, and LR372del were not stably folded (*SI Appendix*, Fig. S3*B*).

PTEN is another key regulator of cellular PIP3 levels by dephosphorylating PIP3. The p85α SH3 and GAP domains involve in p110α-independent regulation of PTEN (17, 18). *PIK3R1* mutations in these domains reduced PTEN protein levels (18, 19). Therefore, we investigated the potential effect of nSH2 domain oncogenic mutants on PTEN protein. As shown in *SI Appendix*, Fig. S4 *A* and *B*, WT p85α increased the protein level and activity of PTEN. All the mutants had the same effect on PTEN as WT p85α. It is unlikely that the oncogenic mechanisms of the tested mutants involve PTEN deregulation.

Next, we determined the phosphorylation levels of signaling proteins of the PI3K pathway. In line with increased PI3K activity, AKT, mTOR, p70-S6K, and S6 were activated in EFE-184 and KLE stable cells (Fig. 2*E*). Unlike the nSH2 truncation mutants that were shown to activate the MAPK pathways in endometrial and ovarian cancer cells (15), this subset of driver mutations had no effect on ERK1/2, JNK, and p38 MAPK (*SI Appendix*, Fig. S4*C*).

nSH2 Domain Driver Mutations Activate Multiple RTKs. Given that the p85α nSH2 domain interacts with pY motifs in RTKs, we investigated the potential effects of nSH2 domain driver mutations on RTK activity. An RTK array that measured the pY levels of 49 human RTKs was performed using EFE-184 cells expressing the driver mutations W333R, G353R, or LR372del (Fig. 3*A*). Interestingly, the pY levels of EGFR, HER2, HER3, c-Met, and IGF-1R were markedly increased in cells expressing W333R, G353R, or LR372del (Fig. 3*B*). In contrast, the phosphorylation levels of HER4 remained unaltered (Fig. 3*C*). A previous study demonstrated that the *PIK3R1* GAP domain mutation R274A activated PDGFR by deregulating Rab5-mediated PDGFR trafficking in mouse fibroblast NIH 3T3 (20). However, our data showed that nSH2 domain driver mutations had no effect on PDGFR levels (Fig. 3*C*) or Rab5 activity (*SI Appendix*, Fig. S4*D*).

Western blotting confirmed the effects of nSH2 domain driver mutations on RTK activation. EGFR, HER2, HER3, c-Met, and IGF-1R were activated in EFE-184 and KLE cells stably expressing W333R, G353R, LR372del, G376R, and K379E (Fig. 4*A*). Because the signal of phosphorylated IGF-1R was weak, we included phosphorylated insulin receptor substrate 1 (IRS-1), a downstream substrate of IGF-1R, as a readout of IGF-1R activity (21). IRS-1 phosphorylation was markedly enhanced by W333R, G353R, LR372del, G376R, and K379E. In contrast, RTKs and IRS-1 were neither activated by the passenger R386G nor by the oncogenic mutant L380del (Fig. 4*A*). Surprisingly, in addition to tyrosine phosphorylation levels, the total protein levels of HER3 and IGF-1R were increased by driver mutations (Fig. 4*A*). In correlation with the lack of an effect on RTK activities, L380del did not increase the levels of HER3 or IGF-1R protein (Fig. 4*A*). These data suggest that the increase in the levels of phosphorylated HER3 and IGF-1R could be due to the increased total HER3 and IGF-1R protein levels, respectively. *PIK3CA* small interfering RNA (siRNA) silencing of p110α neither affected the increased phosphorylation of RTKs and IRS-1 nor total HER3 and IGF-1R levels (*SI Appendix*, Fig. S5), indicating that RTK activation by these driver mutations is p110α-independent.

We established a CRISPR/Cas9-mediated W333R knock-in in the human colon cancer cell line HCT116, because *PIK3R1* mutations frequently manifest in colon cancer patients. W333R was selected for the knock-in due to the availability of the nearby protospacer adjacent motif recognized by Cas9. Successfully edited clones were confirmed via sequencing (*SI Appendix*, Fig. S6*A*). As expected, the three knock-in clones with a heterozygous W333R mutation (designated as CRISPR-W333R-1, -2, and -3) displayed higher viability and clonogenic growth than parental HCT116 or unedited control clones that retained WT *PIK3R1*

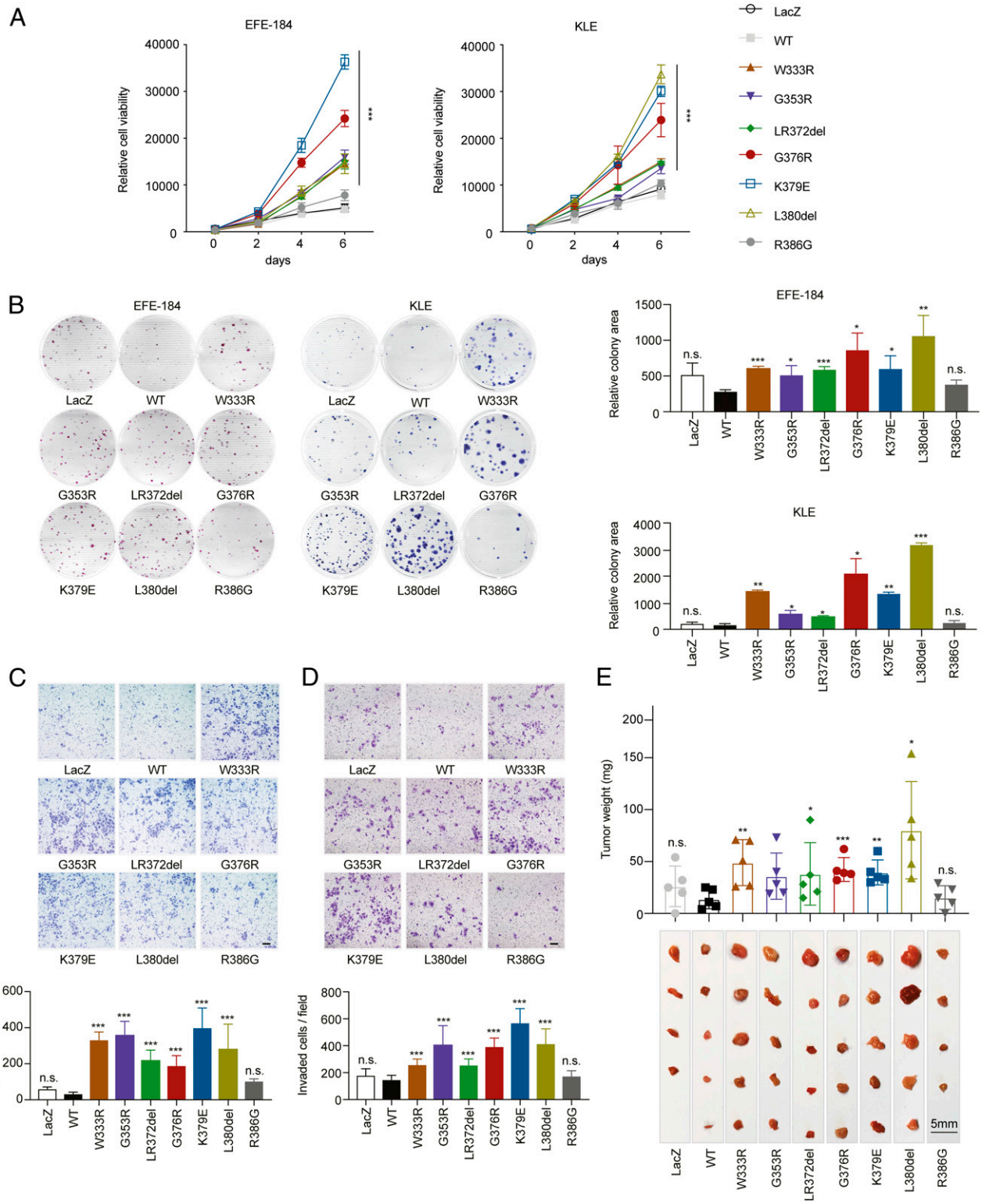

Fig. 1. *PIK3R1* nSH2 domain driver mutations enhance oncogenic phenotypes. EFE-184 or KLE cells stably expressing WT *PIK3R1* or mutations or LacZ were examined for (*A*) cell viability, (*B*) colony formation, (*C*) migration, and (*D*) invasion. (*A*) Cell viability was measured over a period of 6 d. (*B*) Representative images (*Left*) and mean areas (*Right*) of the colonies formed. (*C* and *D*) Representative images (*Upper*) and mean numbers (*Lower*) of migrated or invaded EFE-184 cells in five random fields at 100× magnification (Scale bar, 200 μm). Data are mean ± SD ($n = 3$). (*E*) Stable EFE-184 cells were subcutaneously injected into nude mice ($n = 5$). Tumor nodule weights (*Upper*) and collected nodules (*Lower*) are shown. Error bars represent SD. *$P < 0.05$; **$P < 0.01$; ***$P < 0.001$; and n.s., no significant difference compared with WT using *t* test.

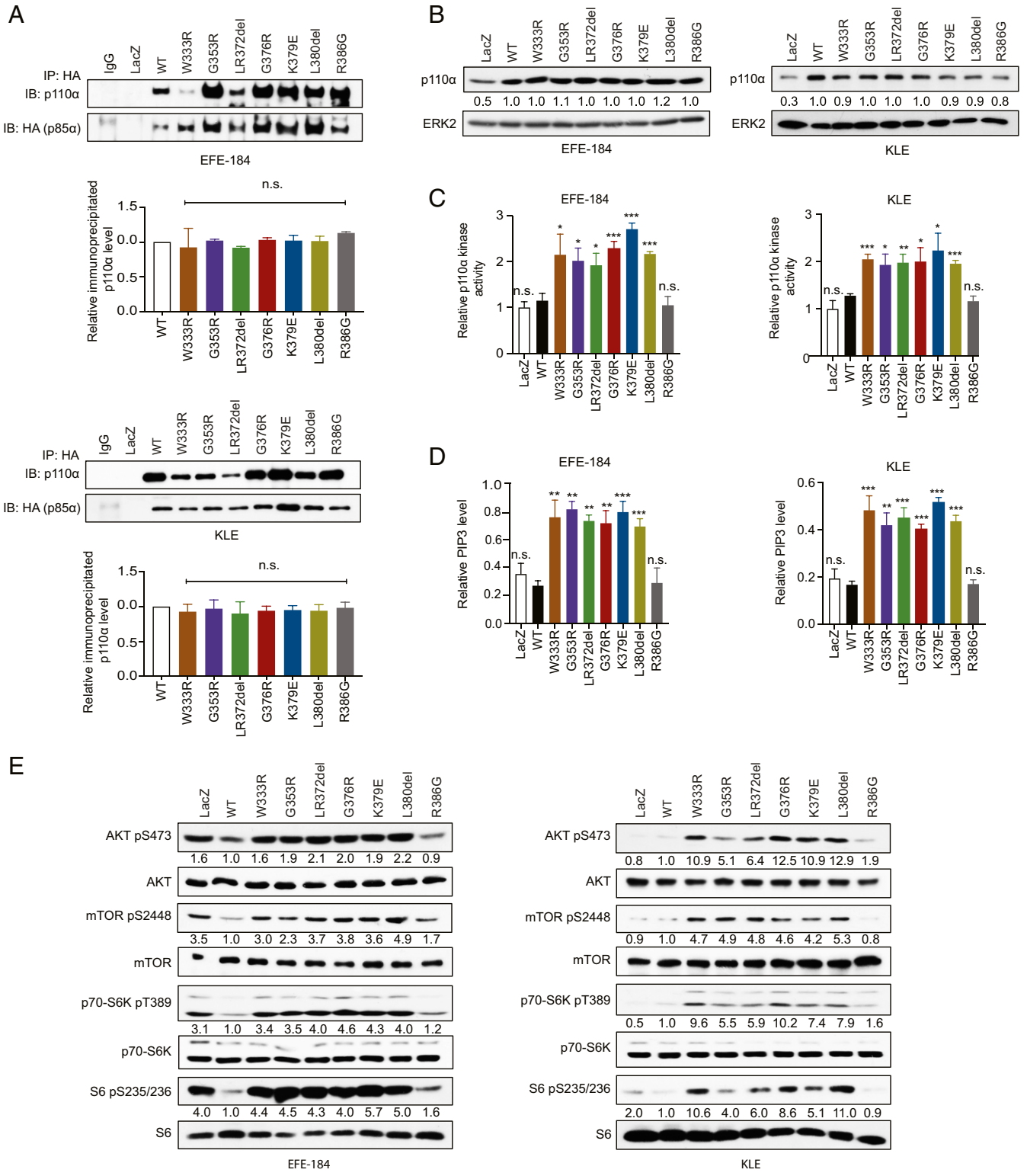

Fig. 2. *PIK3R1* nSH2 domain driver mutations activate p110α and AKT signaling. (*A*) Protein lysates of cells stably expressing HA-tagged WT *PIK3R1* or mutations or LacZ were immunoprecipitated (IP) with anti-HA antibody prior to Western blotting (IB). Immunoprecipitation with rabbit IgG was negative control. (*B*) Protein levels of p110α were examined with ERK2 as loading control. (*C*) p110α protein was IP, and were subjected to PI3K activity assay. (*D*) The lipids in the stable cells were collected for detection. PIP3 levels were normalized with those of PIP2. Data are mean ± SD ($n = 3$). $^*P < 0.05$; $^{**}P < 0.01$; $^{***}P < 0.001$; and n.s., no significant difference compared with WT using *t* test. (*E*) Protein levels of AKT signaling molecules were examined. The bar graphs or numbers below the blots indicate the mean densitometry values normalized to those of HA, ERK2, or the corresponding total protein of three independent experiments.

after the same gene editing procedure (CRISPR-WT-1 and -2) (*SI Appendix*, Fig. S6*B*). Activation of the AKT signaling pathway was evident in the edited cells (Fig. 4*B*). Interestingly, consistent with the endometrial cancer cell models, W333R knock-in cells had elevated levels of phosphorylated RTKs and IRS-1 as well as total levels of HER3 and IGF-1R (Fig. 4*C*).

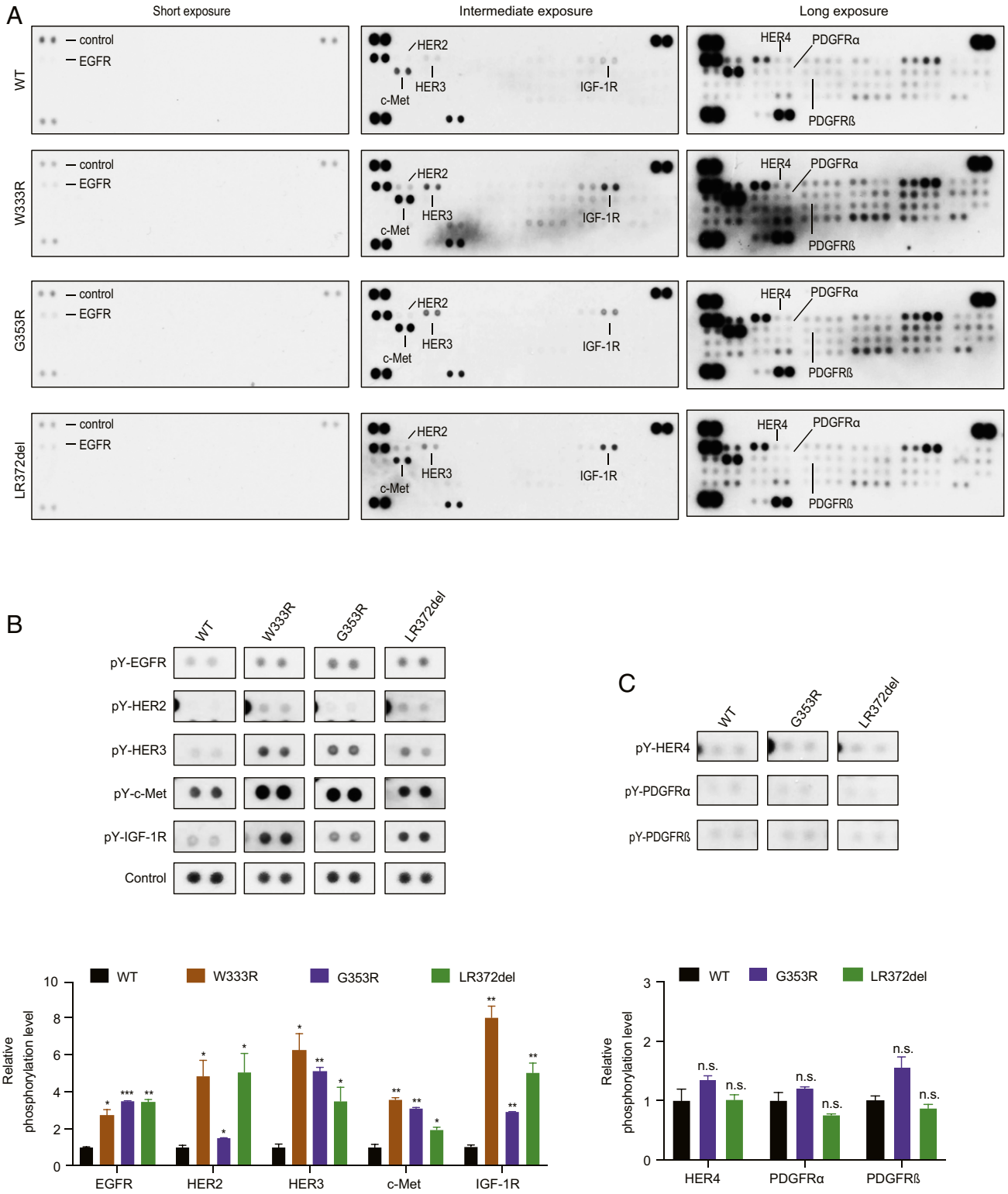

Fig. 3. RTK phosphorylation arrays revealed increased phosphorylation of multiple RTKs by *PIK3R1* nSH2 domain driver mutations. Protein lysates of EFE-184 cells stably expressing WT *PIK3R1* or mutations were subjected to RTK phosphorylation arrays. (*A*) Pictures of the arrays at different exposures. (*B* and *C*) Densitometry values of the duplicate spots on the slides of two different exposures were obtained. Selected spots of the arrays (*Upper*) and fold changes in densitometry values (*Lower*) of the (*B*) activated or (*C*) unaltered RTKs of the mutant cells compared with those of WT are shown. The W333R slide after long exposure had high background and was excluded from analysis. Error bars represent SD. $*P < 0.05$; $**P < 0.01$; $***P < 0.001$; and n.s., no significant difference compared with WT using the *t* test.

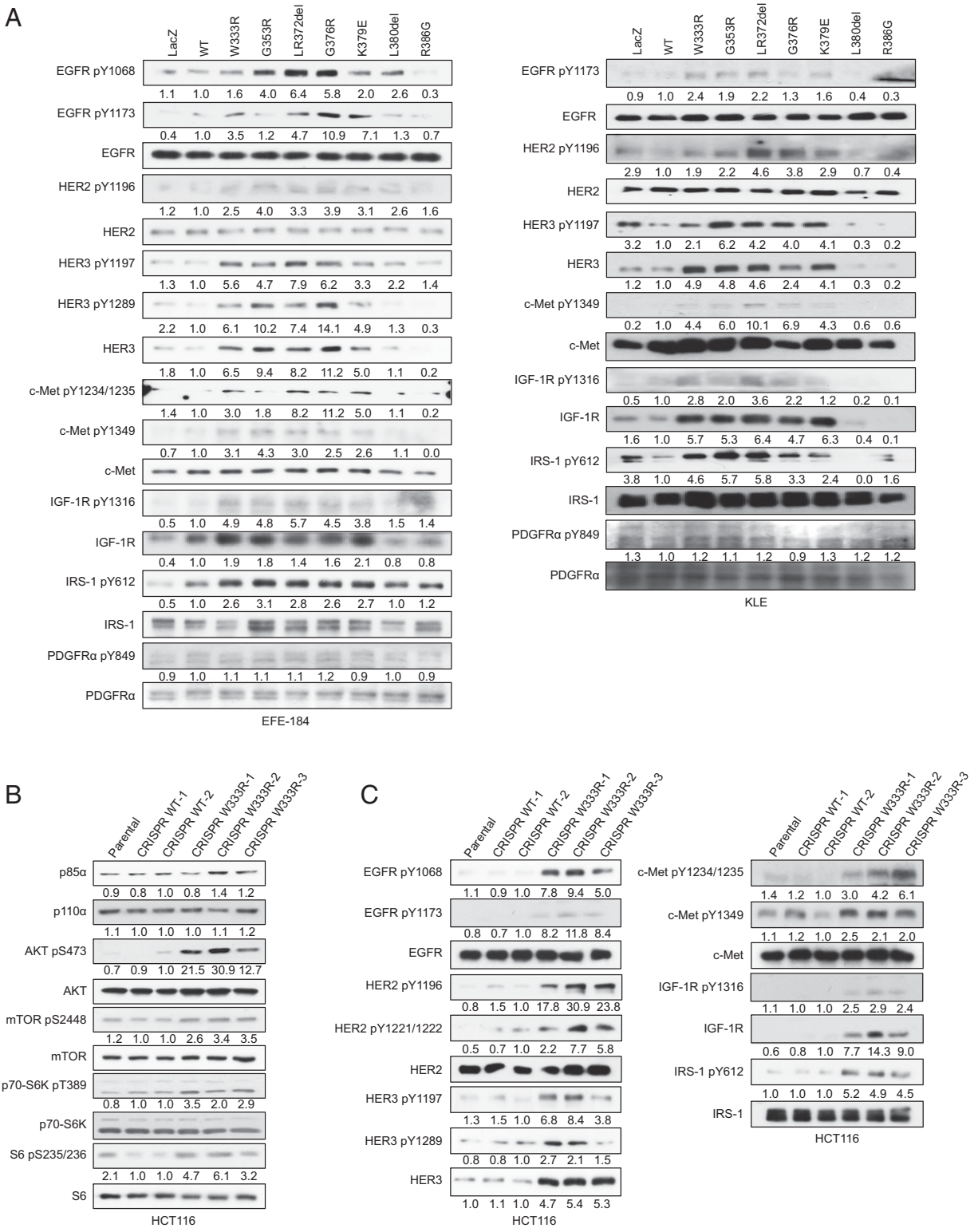

Fig. 4. *PIK3R1* nSH2 domain driver mutations activate EGFR, HER2, HER3, c-Met, and IGF-1R. (*A*) Phosphorylated or total protein levels of the RTKs and IRS-1 in cells stably expressing WT *PIK3R1* or mutations or LacZ were examined by Western blotting. Data of some phosphorylation sites in KLE were unavailable due to undetectable levels. (*B* and *C*) Lysates of parental, CRISPR WT unedited control, or CRISPR *PIK3R1* W333R knock-in HCT-116 cells were subjected to Western blotting. ERK2 was loading control. The numbers below the blots indicate the mean densitometry values of three independent experiments.

nSH2 Domain Driver Mutations Stabilize the HER3 Protein, Leading to the Activation of EGFR, HER2, and c-Met. The HER3 kinase domain has minimal catalytic activity and HER3 signaling primarily occurs through heterodimerization with other RTKs. Upon binding, HER3 acts as an "activator" that allosterically activates its partner RTKs (the "receiver"), which subsequently phosphorylates the receptor tails (22–24). RTKs that dimerize with HER3 include HER family members as well as c-Met and IGF-1R (25–28). We

speculated that the increase in HER3 protein levels leads to increased heterodimerization with receiver RTKs, thereby inducing RTK activation. First, HER3 siRNA abolished the induced phosphorylation of EGFR, HER2, and c-Met, confirming that HER3 mediates the activation of these RTKs (Fig. 5*A*). Moreover, immunoprecipitation revealed the higher abundance of HER3 dimerization with EGFR, HER2, or c-Met (Fig. 5*B*). The induced phosphorylation of IGF-1R and IRS-1 and total IGF-1R was not altered by HER3 knockdown, suggesting that the activation of IGF-1R/IRS-1 is a consequence of an HER3-independent increase in total IGF-1R levels. We also investigated the possibility that IGF-1R/IRS-1 signaling contributes to the RTK activation. Intriguingly, as shown in *SI Appendix*, Fig. S7*A*, *IRS1* siRNA inhibited the activation of c-Met, concordant with previous observation that IGF-1R induces HGF-independent c-Met activation (29). In contrast, *IRS1* knockdown had no impact on the phosphorylation of HER family.

Next, we investigated the mechanisms by which the driver mutations increased total HER3 protein levels. The driver mutations had no impact on *HER3* messenger RNA (mRNA) levels (*SI Appendix*, Fig. S7*B*). Instead, the half-life of HER3 protein was significantly prolonged in the presence of driver mutations (Fig. 5*C* and *SI Appendix*, Fig. S7*C*). This stabilization is likely due to reduced protein degradation because the driver mutations inhibited HER3 ubiquitination (Fig. 5*D*). Further, we observed that immunoprecipitated HER3 displayed increased interaction with the p85α driver mutants (*SI Appendix*, Fig. S8*A*). Reciprocal immunoprecipitation using anti-HA antibody to immunoprecipitate p85α confirmed this finding (*SI Appendix*, Fig. S8*A*). p85α binds to multiple pYXXM motifs of HER3 directly (30, 31), we therefore examined the binding between the mutants with a doubly tyrosine-phosphorylated (2pY) HER3 peptide (DGGGPGGD(pY)AAMGACPASEQG(pY)EEMRAFQG). Our peptide pull-down assay revealed that the 2pY HER3 peptide

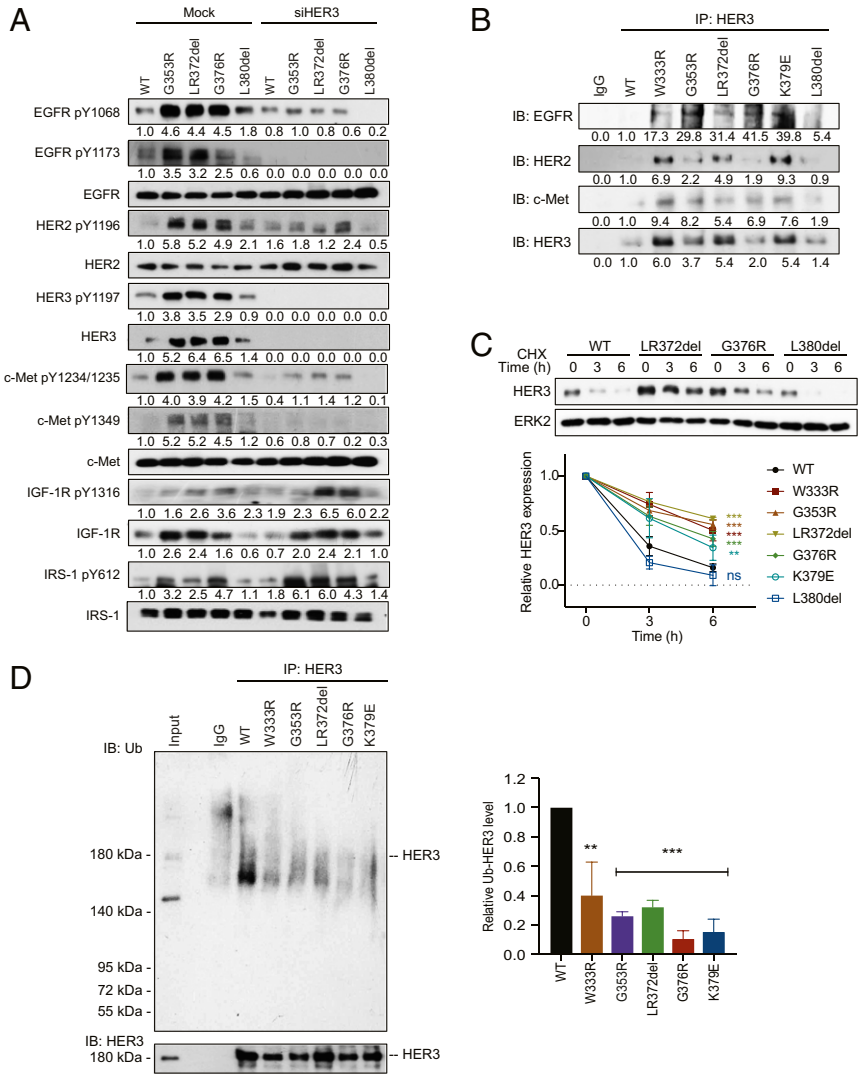

Fig. 5. *PIK3R1* nSH2 domain driver mutations enhance the protein stability of HER3, which mediates the phosphorylation of the other RTKs. (*A*) EFE-184 cells stably expressing WT *PIK3R1* or mutations transfected with *HER3* siRNA or mock for 48 h were subjected to Western blotting. (*B*) Dimerization of HER3 with EGFR, HER2, or c-Met was analyzed by IP using anti-HER3 antibody and Western blotting (IB). Equal amounts of input protein were used for each IP. (*C*) EFE-184 cells were treated with 25 μg/mL cycloheximide (CHX) for the indicated time course. Some blots are shown in *SI Appendix*, Fig. S7*C*. (*D*) Lysates were immunoprecipitated with anti-HER3 antibody. HER3 protein levels were normalized prior to IP by using proportionally different amounts of lysates. Molecular weight standards (kilodalton) and the location of HER3 are indicated. The numbers or bar graphs below the blots indicate the mean densitometry values normalized to those of the corresponding total protein, immunoprecipitated protein, or ERK2 loading control of three independent experiments. Error bars represent SD. $^{**}P < 0.01$; $^{***}P < 0.001$; and n.s., no significant difference compared with WT using the *t* test.

bound stronger to W333R, G353R, LR372del, G376R, and K379E than to WT p85α (*SI Appendix*, Fig. S8*B*).

To test whether the mutated nSH2 domains have stronger pY peptide interaction, we repeated this binding assay with purified recombinant nSH2 domains. In contrast to mutants in the context of full-length p85α protein, the recombinant domains either had an unchanged affinity for the 2pY HER3 peptide (G376R, K379E, and L380del), or had markedly lost binding affinity (W333R, G353R, and LR372del) compared with WT p85α (*SI Appendix*, Fig. S8*C*). These results were confirmed by isothermal titration calorimetry (ITC) (*SI Appendix*, Fig. S8*D*). The nSH2 mutants with the most markedly lost affinity for the HER3 peptides were those identified as structurally destabilized using DSF (*SI Appendix*, Fig. S3*B*). Conversely, G376R and K379E affect surface residues that may tolerate these substitutions. The observation that L380del neither decreased the nSH2 stability nor the pY peptide affinity was unexpected, given its location within the peptide binding site (*SI Appendix*, Fig. S3*A*). Taken together, our data suggest that those driver mutants that increase HER3 protein levels do so by protecting HER3 from degradation. However, the effect does not result from an increased affinity of the mutated nSH2 domains toward the HER3 pY motifs.

Driver Mutations Sensitize Cancer Cells to AKT and HER Family Inhibitors. Cells expressing the six p85α driver mutations had higher AKT phosphorylation levels and were more sensitive to AKT inhibitor (MK-2206) than those expressing WT *PIK3R1* or the passenger R386G (Fig. 6 *A* and *B*). Because the half inhibitory concentration could not be achieved in some conditions, the area under the dose–response curve (AUC) was calculated to represent drug response (Fig. 6*B*). The nSH2 domain mutations do not confer sensitivity to EGFR inhibitor erlotinib (Fig. 6*A*). Building on our observations of HER2 and HER3 activation in driver mutation-expressing cells, we performed drug-response assays using lapatinib (EGFR and HER2 inhibitor) and AZD-8931 (EGFR, HER2, and HER3 inhibitor). Cells with the five driver mutations that caused RTK activation (W333R, G353R, LR372del, G376R, and K379E) were more sensitive to lapatinib and AZD-8931 than cells with LacZ, WT, and the passenger R386G (Fig. 6 *A* and *B*). In line with minimal changes in RTK signaling, L380del-expressing cells did not show better response to HER family inhibitors (Fig. 6 *A* and *B*).

Dual Inhibition of AKT and the HER Family Results in Synergism in Driver Mutation-Expressing Cells. We assessed the combined effects of inhibiting both the AKT and HER family pathways. Driver mutation-expressing cells or WT cells were treated with AKT or HER family inhibitors alone or in combination with serial concentrations of these inhibitors at a fixed molar ratio. A pronounced synergistic antitumor effect was achieved following combined treatment with MK-2206 and AZD-8931 in cells expressing the five driver mutations (W333R, G353R, LR372del, G376R, and K379E) (Fig. 7 *A* and *B*). We also observed a similar

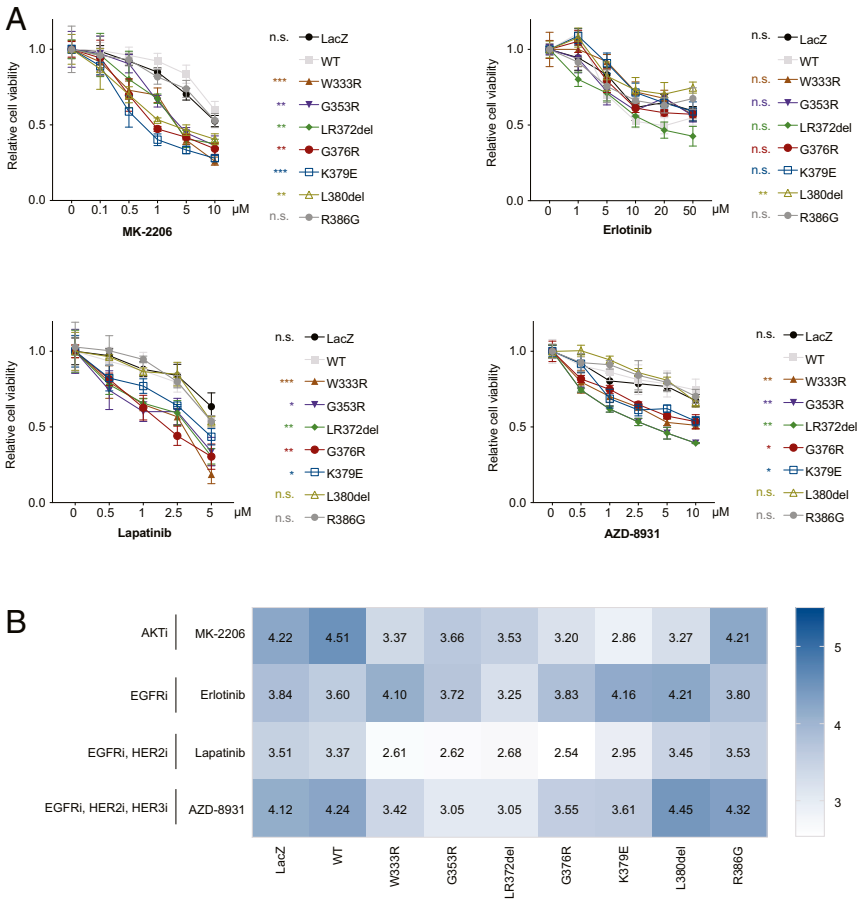

Fig. 6. *PIK3R1* nSH2 domain driver mutations render cells sensitive to AKT inhibitor and HER family inhibitors. EFE-184 cells stably expressing WT *PIK3R1* or mutations or LacZ were treated with the inhibitors for 72 h. (*A*) Dose–response curves of the inhibitors. *P* values were calculated using values at the highest doses. Data are mean ± SD ($n = 3$). *$P < 0.05$; **$P < 0.01$; ***$P < 0.001$; and n.s., no significant difference compared with WT using the *t* test. (*B*) Heatmap of the AUC values of each inhibitor.

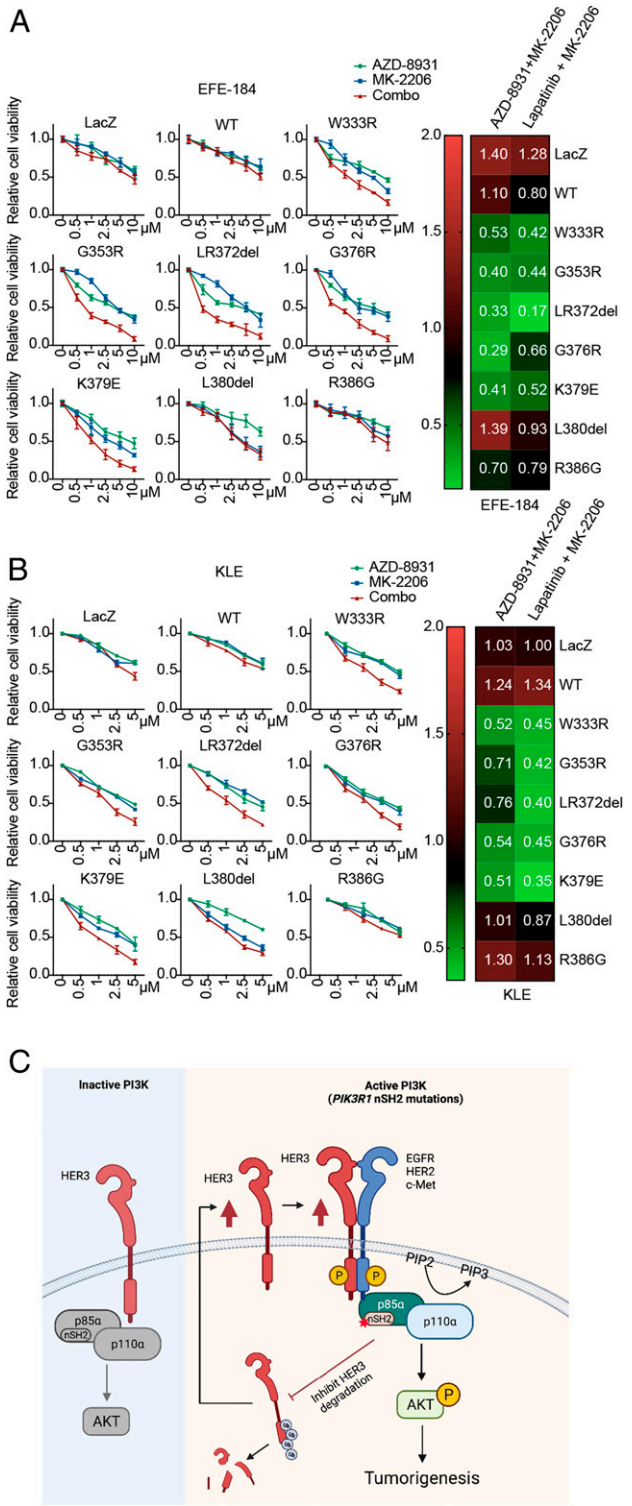

Fig. 7. Cotargeting AKT and HER family induces synergism in cells expressing the *PIK3R1* nSH2 domain driver mutations. (*A*) EFE-184 or (*B*) KLE cells stably expressing WT *PIK3R1* or mutations or LacZ were treated with MK-2206, AZD-8931, or lapatinib alone or in combination with serial concentrations at a fixed molar ratio. (*Left*) Dose–response curves of MK-2206 and AZD-8931. Data are mean ± SD ($n = 3$). (*Right*) Combination Index values of the drug combination were calculated using the Chou–Talalay method, and values at the highest doses are presented. (*C*) Proposed mechanistic model underlying the activation of p110α by the *PIK3R1* nSH2 domain driver mutations: apart from weakening the inhibitory interaction with p110α, the mutants lead to increased abundance of HER3 protein, which dimerizes with and activates EGFR, HER2, and c-Met.

synergistic effect in cells cotreated with MK2206 and lapatinib (Fig. 7 *A* and *B* and *SI Appendix*, Fig. S9). The synergistic antitumor effects of these drug combinations were not observed in cells expressing LacZ, WT, L380del, or R386G.

Discussion

The p85α nSH2 domain establishes an inhibitory contact with p110, which is outcompeted by binding to pYXXM motifs in RTKs (3, 8). Herein, we identify six nSH2 variants that weaken these inhibitory contacts, either by directly affecting p110 binding (G376R, K379E, and L380del) or by destabilizing the nSH2 domain fold (W333R, G353R, and LR372del). In line with our results, K379E has been previously proposed to be oncogenic by disrupting the inhibitory salt bridge interaction between p85α and E545 in the p110α helical domain (4).

In addition, we observed that five of the six nSH2 domain driver mutations (W333R, G353R, LR372del, G376R, and K379E) activated multiple RTKs through p110α-independent increases in the protein levels of HER3 and IGF-1R (Fig. 7*C*). Among the five activated RTKs, HER3, c-Met, and IGF-1R contain YXXM motifs that bind to the p85α nSH2 domain. In contrast, EGFR and HER2 lack the YXXM motif and do not directly bind to p85α. Interestingly, the binding between p85α and HER3 was shown to be stronger than that between p85α and other HER family members or c-Met (32), inferring that HER3 is a preferred partner of p85α. The driver mutants enhanced HER3 protein levels through inhibiting HER3 degradation. At present, our data cannot explain the regulation of IGF-1R protein by the mutations. Although heterotrimers comprising HER2, HER3, and IGF-1R have been observed in trastuzumab-resistant breast cancer cells (28), our data suggest that HER3 does not mediate IGF-1R regulation in p85α mutant cells. Further, the regulation of RTKs by the nSH2 mutants is selective because the mutants did not stabilize c-Met despite the fact that p85α can directly bind to c-Met.

Our data show that the increase in HER3 protein stability induced by driver mutations elevated the abundance of heterodimeric EGFR/HER3, HER2/HER3, and c-Met/HER3. Our observation that HER3 did not activate HER4 can be explained by previous observations that HER3 is a poor activator of HER4 (33) and that HER3/HER4 heterodimer is an inhibitory interaction (34). Thus, our data present the general mechanism to explain the mutants' effect on the RTKs. However, the molecular details remain to be elucidated, because increased HER3 binding was not observed with recombinant nSH2 domain mutants. The difference in HER3 binding between mutants in the context of the full-length p85α and the isolated nSH2 domains may indicate the involvement of other p85α domains. For examples, the cSH2 domain also binds to pYXXM motifs (35) and the p85α SH3 domain, which itself does not bind HER3, enhances HER3 binding by p85α (30, 31). The presence of the nSH2 mutations in the context of cell-derived full-length p85α may lead to alterations of intramolecular or intermolecular association of p85α that favor HER3 binding. The mutations' effect on RTKs cannot be simply explained by the relief of p110α inhibitory interaction, because this effect was independent of p110α and it was not produced by the L380del mutant.

HER3 overexpression is frequently observed in malignancies, including endometrial and colon cancers (36–38). HER3 is an oncogene associated with tumorigenesis and poor patient prognosis (37, 39–41). The nSH2 domain driver mutant cells displayed characteristics resembling HER3-overexpressing cells. First, cells with high HER3 expression showed activation of the PI3K pathway but not the MAPK pathway (42, 43). Second, therapeutically, HER3 overexpression correlates with responses to the dual EGFR/HER2 inhibitor lapatinib across 19 endometrial cancer cell lines (44). We also observed that nSH2 driver mutations did not alter the sensitivity of cells toward the EGFR

inhibitor erlotinib. In line with this finding, HER3 activation might cause erlotinib resistance by dimerizing with other RTKs to induce compensatory signaling (26).

In summary, this study revealed the oncogenic mechanisms of several patient-derived nSH2 domain driver mutations and identified responses to drugs targeting the activated molecules. Five (W333R, G353R, G376R, K379E, and L380del) of the six driver mutations were detected in more than one cancer patient (*SI Appendix*, Fig. S1*A*). The cancer types with these mutations detected include that of breast, colon, and skin and most frequently endometrial cancer and glioblastoma [Catalogue Of Somatic Mutations In Cancer (COSMIC) database] (45). Exploitation of these mutations for cancer therapeutics warrants further investigation.

Materials and Methods

A detailed description of the materials and methods can be found in *SI Appendix*.

Cell Lines and Transfection. KLE and HCT-116 cells were obtained from American Type Culture Collection (Manassas), and EFE-184 cells were obtained from DSMZ-German Collection of Microorganisms and Cell Cultures (Braunschweig, Germany). The cell culture conditions, generation of stable cells and knock-in cells, and information of plasmids and siRNA are provided in *SI Appendix*.

Phenotypic Assays. In colony formation assay, 800 cells were seeded into 6-well plate and were cultured up to 21 d. In the viability assay, 1,000 cells were seeded in triplicate into a 96-well plate. Cell viability was measured at indicated time points with resazurin. In cell migration and invasion assays, 3×10^4 cells were seeded into Matrigel-coated (invasion) or -uncoated (migration) inserts. After 24 h, cells were fixed and stained with crystal violet. In the in vivo tumorigenicity experiment, 5×10^6 cells were subcutaneously injected into female athymic nude mouse ($n = 5$ each group; Charles River Lab). Tumor nodules were collected after 8 wk (details in *SI Appendix*).

Western Blotting, Immunoprecipitation, Peptide Pull-Down Assay, and Phospho-RTK Array. Protein lysates were prepared using the corresponding lysis buffers. Equal amounts of protein were subjected to Western blotting or phospho-RTK array. In immunoprecipiation or pull-down experiments, protein lysates were incubated with primary antibody or peptide. The eluents were analyzed by Western blotting. Detailed procedures and information of the antibodies are provided in *SI Appendix*.

Production of Recombinant Proteins, DSF, and ITC. Recombinant nSH2 domain proteins were expressed in *Escherichia coli* Bl21 (DE3) cells. The purified proteins were subjected to DSF and ITC. DSF experiments were performed on C1000 Touch thermal cycler CFX96 Real-Time system (Bio-Rad) in conjunction with SYPRO Orange 5000X dye (Invitrogen). ITC experiments were performed on a MicroCal ITC200 (GE HealthCare). Refer to *SI Appendix* for details.

Drug Response Assay. Cells seeded at a density of 1,000 cells/well in a 96-well plate were treated with serial diluted single or combined inhibitors for 72 h. Viable cells were detected with resazurin (details in *SI Appendix*). The AUC values were obtained using the GraphPad Prism 8 software (La Jolla). The synergistic effects of the drug combinations were quantified using the CompuSyn Software (Biosoft, Version 2.1)

PI3K Activity Assay and PIP3/PIP2 Quantification. To measure in vitro kinase activity, the immunoprecipitated p110α protein was incubated with PIP2 substrate to generate PIP3. The amount of generated PIP3 was detected at 450 nm. To measure cellular PIP3 and PIP2 levels, total lipids were extracted using ice-cold 0.5 M trichloroacetic acid prior to extraction of acidic lipids in the organic phase (details in *SI Appendix*).

Statistical Analyses. All experiments were performed three times. Results are presented as mean ± SD. *P* values were calculated using the Student's unpaired two-tailed *t* test with GraphPad Prism. *P* values < 0.05 were considered statistically significant.

Data Availability. All study data are included in the article and/or *SI Appendix*.

ACKNOWLEDGMENTS. This study was supported by the National Natural Science Foundation of China (Grants 81703066 and 82022078 to L.W.T.C.). S.T.A. and A.A. were supported by King Abdullah University of Science and Technology (KAUST) through the baseline fund and Awards FCC/1/1976-25 and REI/1/4446-01 from the Office of Sponsored Research. We thank I. Salem, R. Ramakrishnan, and S. Hong for their comments on the manuscript, as well as Huma Khurram and the KAUST Bioscience Core Lab for assistance with the mass spectrometry.

1. R. L. Grossman *et al.*, Toward a shared vision for cancer genomic data. *N. Engl. J. Med.* **375**, 1109–1112 (2016).
2. L. W. Cheung, G. B. Mills, Targeting therapeutic liabilities engendered by *PIK3R1* mutations for cancer treatment. *Pharmacogenomics* **17**, 297–307 (2016).
3. J. Yu, C. Wjasow, J. M. Backer, Regulation of the p85/p110alpha phosphatidylinositol 3′-kinase. Distinct roles for the n-terminal and c-terminal SH2 domains. *J. Biol. Chem.* **273**, 30199–30203 (1998).
4. M. Sun, P. Hillmann, B. T. Hofmann, J. R. Hart, P. K. Vogt, Cancer-derived mutations in the regulatory subunit p85alpha of phosphoinositide 3-kinase function through the catalytic subunit p110alpha. *Proc. Natl. Acad. Sci. U.S.A.* **107**, 15547–15552 (2010).
5. B. S. Jaiswal *et al.*, Somatic mutations in p85alpha promote tumorigenesis through class IA PI3K activation. *Cancer Cell* **16**, 463–474 (2009).
6. S. N. Quayle *et al.*, Somatic mutations of *PIK3R1* promote gliomagenesis. *PLoS One* **7**, e49466 (2012).
7. H. Wu *et al.*, Regulation of Class IA PI 3-kinases: C2 domain-iSH2 domain contacts inhibit p85/p110alpha and are disrupted in oncogenic p85 mutants. *Proc. Natl. Acad. Sci. U.S.A.* **106**, 20258–20263 (2009).
8. M. S. Miller, P. E. Thompson, S. B. Gabelli, Structural determinants of isoform selectivity in PI3K inhibitors. *Biomolecules* **9**, 82 (2019).
9. N. Miled *et al.*, Mechanism of two classes of cancer mutations in the phosphoinositide 3-kinase catalytic subunit. *Science* **317**, 239–242 (2007).
10. X. Zhang *et al.*, Structure of lipid kinase p110β/p85β elucidates an unusual SH2-domain-mediated inhibitory mechanism. *Mol. Cell* **41**, 567–578 (2011).
11. L. Chen *et al.*, Characterization of *PIK3CA* and *PIK3R1* somatic mutations in Chinese breast cancer patients. *Nat. Commun.* **9**, 1357 (2018).
12. T. Rordorf-Nikolic, D. J. Van Horn, D. Chen, M. F. White, J. M. Backer, Regulation of phosphatidylinositol 3′-kinase by tyrosyl phosphoproteins. Full activation requires occupancy of both SH2 domains in the 85-kDa regulatory subunit. *J. Biol. Chem.* **270**, 3662–3666 (1995).
13. J. Y. Lee, Y. H. Chiu, J. Asara, L. C. Cantley, Inhibition of PI3K binding to activators by serine phosphorylation of PI3K regulatory subunit p85alpha Src homology-2 domains. *Proc. Natl. Acad. Sci. U.S.A.* **108**, 14157–14162 (2011).
14. P. K. Ng *et al.*, Systematic functional annotation of somatic mutations in cancer. *Cancer Cell* **33**, 450–462.e10 (2018).
15. L. W. Cheung *et al.*, Naturally occurring neomorphic *PIK3R1* mutations activate the MAPK pathway, dictating therapeutic response to MAPK pathway inhibitors. *Cancer Cell* **26**, 479–494 (2014).
16. J. Yu *et al.*, Regulation of the p85/p110 phosphatidylinositol 3′-kinase: Stabilization and inhibition of the p110alpha catalytic subunit by the p85 regulatory subunit. *Mol. Cell. Biol.* **18**, 1379–1387 (1998).
17. R. B. Chagpar *et al.*, Direct positive regulation of PTEN by the p85 subunit of phosphatidylinositol 3-kinase. *Proc. Natl. Acad. Sci. U.S.A.* **107**, 5471–5476 (2010).
18. L. W. Cheung *et al.*, Regulation of the PI3K pathway through a p85α monomer-homodimer equilibrium. *eLife* **4**, e06866 (2015).
19. P. Mellor *et al.*, Patient-derived mutations within the N-terminal domains of p85α impact PTEN or Rab5 binding and regulation. *Sci. Rep.* **8**, 7108 (2018).
20. M. D. Chamberlain *et al.*, Deregulation of Rab5 and Rab4 proteins in p85R274A-expressing cells alters PDGFR trafficking. *Cell. Signal.* **22**, 1562–1575 (2010).
21. M. G. Myers Jr *et al.*, IRS-1 is a common element in insulin and insulin-like growth factor-I signaling to the phosphatidylinositol 3′-kinase. *Endocrinology* **132**, 1421–1430 (1993).
22. H. H. Kim, U. Vijapurkar, N. J. Hellyer, D. Bravo, J. G. Koland, Signal transduction by epidermal growth factor and heregulin via the kinase-deficient ErbB3 protein. *Biochem. J.* **334**, 189–195 (1998).
23. M. A. Olayioye, R. M. Neve, H. A. Lane, N. E. Hynes, The ErbB signaling network: Receptor heterodimerization in development and cancer. *EMBO J.* **19**, 3159–3167 (2000).
24. A. Citri, K. B. Skaria, Y. Yarden, The deaf and the dumb: The biology of ErbB-2 and ErbB-3. *Exp. Cell Res.* **284**, 54–65 (2003).
25. B. van Lengerich, C. Agnew, E. M. Puchner, B. Huang, N. Jura, EGF and NRG induce phosphorylation of HER3/ERBB3 by EGFR using distinct oligomeric mechanisms. *Proc. Natl. Acad. Sci. U.S.A.* **114**, E2836–E2845 (2017).
26. J. A. Engelman *et al.*, MET amplification leads to gefitinib resistance in lung cancer by activating ERBB3 signaling. *Science* **316**, 1039–1043 (2007).
27. C. Yun *et al.*, Essential role of Her3 in two signaling transduction patterns: Her2/Her3 and MET/Her3 in proliferation of human gastric cancer. *Mol. Carcinog.* **54**, 1700–1709 (2015).
28. X. Huang *et al.*, Heterotrimerization of the growth factor receptors erbB2, erbB3, and insulin-like growth factor-I receptor in breast cancer cells resistant to herceptin. *Cancer Res.* **70**, 1204–1214 (2010).

29. A. Varkaris *et al*., Ligand-independent activation of MET through IGF-1/IGF-1R signaling. *Int. J. Cancer* **133**, 1536–1546 (2013).
30. N. J. Hellyer, K. Cheng, J. G. Koland, ErbB3 (HER3) interaction with the p85 regulatory subunit of phosphoinositide 3-kinase. *Biochem. J.* **333**, 757–763 (1998).
31. A. Suenaga *et al*., Novel mechanism of interaction of p85 subunit of phosphatidylinositol 3-kinase and ErbB3 receptor-derived phosphotyrosyl peptides. *J. Biol. Chem.* **280**, 1321–1326 (2005).
32. K. K. Leung *et al*., Enhanced prediction of Src homology 2 (SH2) domain binding potentials using a fluorescence polarization-derived c-Met, c-Kit, ErbB, and androgen receptor interactome. *Mol. Cell. Proteomics* **13**, 1705–1723 (2014).
33. J. Monsey, W. Shen, P. Schlesinger, R. Bose, Her4 and Her2/neu tyrosine kinase domains dimerize and activate in a reconstituted in vitro system. *J. Biol. Chem.* **285**, 7035–7044 (2010).
34. N. Jura, Y. Shan, X. Cao, D. E. Shaw, J. Kuriyan, Structural analysis of the catalytically inactive kinase domain of the human EGF receptor 3. *Proc. Natl. Acad. Sci. U.S.A.* **106**, 21608–21613 (2009).
35. S. Inaba *et al*., Crystal structures and thermodynamic analysis reveal distinct mechanisms of CD28 phosphopeptide binding to the Src homology 2 (SH2) domains of three adaptor proteins. *J. Biol. Chem.* **292**, 1052–1060 (2017).
36. R. Srinivasan, E. Benton, F. McCormick, H. Thomas, W. J. Gullick, Expression of the c-erbB-3/HER-3 and c-erbB-4/HER-4 growth factor receptors and their ligands, neuregulin-1 alpha, neuregulin-1 beta, and betacellulin, in normal endometrium and endometrial cancer. *Clin. Cancer Res.* **5**, 2877–2883 (1999).
37. A. Beji, D. Horst, J. Engel, T. Kirchner, A. Ullrich, Toward the prognostic significance and therapeutic potential of HER3 receptor tyrosine kinase in human colon cancer. *Clin. Cancer Res.* **18**, 956–968 (2012).
38. S. T. Lee-Hoeflich *et al*., A central role for HER3 in HER2-amplified breast cancer: Implications for targeted therapy. *Cancer Res.* **68**, 5878–5887 (2008).
39. H. Liang *et al*., Whole-exome sequencing combined with functional genomics reveals novel candidate driver cancer genes in endometrial cancer. *Genome Res.* **22**, 2120–2129 (2012).
40. B. Tanner *et al*., ErbB-3 predicts survival in ovarian cancer. *J. Clin. Oncol.* **24**, 4317–4323 (2006).
41. F. Lédel, K. Stenstedt, M. Hallström, P. Ragnhammar, D. Edler, HER3 expression in primary colorectal cancer including corresponding metastases in lymph node and liver. *Acta Oncol.* **54**, 480–486 (2015).
42. D. C. Kirouac *et al*., HER2+ cancer cell dependence on PI3K vs. MAPK signaling axes is determined by expression of EGFR, ERBB3 and CDKN1B. *PLOS Comput. Biol.* **12**, e1004827 (2016).
43. Y. Huang *et al*., Development of a test that measures real-time HER2 signaling function in live breast cancer cell lines and primary cells. *BMC Cancer* **17**, 199 (2017).
44. G. E. Konecny *et al*., Activity of lapatinib a novel HER2 and EGFR dual kinase inhibitor in human endometrial cancer cells. *Br. J. Cancer* **98**, 1076–1084 (2008).
45. J. G. Tate *et al*., COSMIC: The catalogue of somatic mutations in cancer. *Nucleic Acids Res.* **47** (D1), D941–D947 (2019).